Multivalent Mg 2+ -, Zn 2+ -, and Ca 2+ -Ion Intercalation Chemistry in a Disordered Layered Structure

Seongkoo Kang, Kyle G Reeves, Toshinari Koketsu, Jiwei Ma, Olaf J Borkiewicz, Peter Strasser, Alexandre Ponrouch, Damien Dambournet

Multivalent Mg^{2+}, Zn^{2+} and Ca^{2+} Ion Intercalation Chemistry in a Disordered Layered Structure

Seongkoo Kang[a,b‡], Kyle G. Reeves[a,b‡], Toshinari Koketsu[c], Jiwei Ma[d], Olaf J. Borkiewicz[e], Peter Strasser[c], Alexandre Ponrouch[f,g] and Damien Dambournet[a,b*]

[a] Sorbonne Université, CNRS, Physico-chimie des électrolytes et nano-systèmes interfaciaux, PHENIX, F-75005 Paris, France

[b] Réseau sur le Stockage Electrochimique de l'Energie (RS2E), FR CNRS 3459, 80039 Amiens, France

[c] The Electrochemical Energy, Catalysis, and Materials Science Laboratory, Department of Chemistry, Chemical Engineering Division, Technical University Berlin, 10623 Berlin, Germany

[d] Institute of New Energy for Vehicles, School of Materials Science and Engineering, Tongji University, Shanghai 201804, China.

[e] X-ray Science Division, Advanced Photon Source, Argonne National Laboratory, 9700 South Cass Avenue, Argonne, Illinois 60439, United States

[f] Institut de Ciència de Materials de Barcelona (ICMAB-CSIC), Campus UAB, 08193 Bellaterra, Spain

[g] ALISTORE – European Research Institute, CNRS FR3104, Hub de l'Energie, 15 Rue Baudelocque, 80039 Amiens, France.

KEYWORDS. Disordered structure, lepidocrocite, perovskite, defects, multivalent, rechargeable batteries.

ABSTRACT: The development of practical multivalent-ion batteries critically depends on the identification of suitable positive electrode materials. To gain a better understanding of the intercalation chemistry of multivalent ions, model frameworks can be used to study the distinct specificities of possible multivalent ions, thus expanding our knowledge on the emerging "Beyond Li battery" technology. Here, we compare the intercalation chemistry of Mg^{2+}, Zn^{2+} and Ca^{2+} ions into a disordered layered-type structure featuring water interlayers and cationic vacancies as possible host sites. The thermodynamics of cation-inserted reactions performed on the model structure indicated that these reactions are thermodynamically favourable with Zn^{2+} being the least stable ion. Galvanostatic measurements confirmed that the structure is inactive toward Zn^{2+} intercalation while Mg^{2+} can be reversibly inserted (0.37 Mg^{2+} per formula unit) with minor changes of the atomic arrangement as demonstrated by pair distribution function analysis. Moreover, we demonstrate that non-solvated Mg^{2+} was intercalated in the structure. Finally, the intercalation of Ca^{2+} performed at 100 °C with $Ca(BF_4)_2$ in propylene carbonate, induced the collapse of the layered structure releasing water molecules that contribute to the degradation of the electrolyte as revealed by the presence of CaF_2 at the electrode level. The decomposition of the structure led to the formation of an electrochemically active phase featuring strong long-range disorder, yet short-range order close to that found in perovskite structures, particularly with corner-shared TiO_6 octahedra. We, hence, hypothesize that defective $CaTiO_3$-based perovskite could be explored as viable cathode materials for rechargeable Ca-based batteries.

The modern-day search for new materials to be used in rechargeable batteries has focused on various components of the devices including the electrolyte and compositions of the positive and negative electrodes. An additional consideration is the ion that travels between electrodes. Given the limited amount of available lithium, previous work has explored the possibility of using other monovalent ions such as Na^+ or K^+ instead.[1] An alternative approach takes advantage of the earth crust's abundant multivalent (MV) ions such as Mg^{2+} and Ca^{2+}, or Zn^{2+} although it is barely more abundant than Li^+, as the charge-carrying species.[2–8] In a system which uses a metal anode, multivalent ions take advantage of a multi-electron processes leading to a corresponding increase in the volumetric energy density (Table 1). The proper plating/stripping of the metal in a selected electrolyte without the formation of dendrite is a mandatory step toward the realization of beyond lithium-ion batteries with enhanced safety.

However, while the energy density of a battery can, in principle, be significantly enhanced using Mg, Ca or Zn metal anodes, the development of positive electrode materials that can accommodate these ions is still in its early stages.[9,10] The difficulty lies in the slow solid-state diffusion of MV ions within the structure caused by the strong Coulombic interactions with the anionic sublattice. To account for this, the polarizing power (ratio between the charge and the square of the ionic radius: Z/r^2) reflects the ability of a cation to attract and distort the electron cloud of a nearby anion (Table 1). Considering a six-fold coordination number (CN), the ranking goes $Li^+ < Ca^{2+} < Zn^{2+} < Mg^{2+}$ indicating that the greater challenges

may be expected in developing beyond-lithium ion rechargeable batteries. This trend, however, does not take into account the specific behaviour of these ions within electrode structures, an environment unlike bulk solvation in which ions are confined. These potential new generations of batteries require more investigation to better understand the stability of each ion species when intercalated into the electrode material.[9] Model frameworks such as layered structures are particularly interesting to explore due to the ability of these materials to accommodate ions with a range of sizes and the possible variability in the coordination environment for intercalated species.[11] Moreover, highly defective structures were shown to favour the diffusion of MV ions.[12,13] Herein, we embark on comparing the intercalation chemistry of MV ions within a disordered layered structure featuring interlayer water molecules and cationic vacancies both potentially acting as host sites. DFT-calculations on simplified structural model were primarily used to access the thermodynamic properties and to provide structural insights into the properties of inserted cations highlighting noticeable differences. Although the comparison between ions is constrained by the specific electrochemical features of each cell (e.g. the electrolyte associated with each multivalent ion), this work provides fundamental insights into different intercalation chemistries.

Table 1. Characteristics of different charge carriers.

Characteristics	Li^+	Ca^{2+}	Zn^{2+}	Mg^{2+}
Earth crust abundance (ppm)	20	41,000	75	23,300
Volumetric capacity (mAh/cm^3)	2,061	2,073	5,854	3,832
Shannon's ionic radii (Å) (CN*=VI)	0.76	1.00	0.74 0.60**	0.72
Polarizing power (Z/r^2) ($Å^{-2}$)	1.73	2.00	3.65 5.55**	3.85

*CN: Coordination number

** CN of Zn^{2+} in ZnO is IV.

EXPERIMENTAL SECTION

Synthesis. X-ray amorphous sample with a local lepidocrocite-type layered structure containing a high concentration of titanium vacancies was synthesized by a sol-gel process as previously reported.[14] Briefly, a solution containing 4 mL of titanium (IV) isopropoxide (> 97 %, Sigma-Aldrich), 25.19 mL of isopropanol (Alfa Aesar) and 0.81 mL of ultrapure water, was placed in a Teflon-lined container sealed in the autoclave. The mixture underwent thermally activated precipitation at 90 °C for 12 h. The obtained white precipitate was washed several times with ethanol (> 96 %), collected by centrifugation and further dried at 80 °C overnight. The determination of the chemical formula led to $Ti_{1.5}\square_{0.5}O_2(OH)_2{\cdot}nH_2O$ ($\square$ = Ti^{4+} vacancy, n~0.55) where 25% Ti^{4+} replaced by vacancies to compensate the charge difference due to the substitution of divalent O^{2-} by monovalent OH^- groups.

Electrochemistry. The electrochemical activity of $Ti_{1.5}\square_{0.5}O_2(OH)_2{\cdot}nH_2O$ versus Mg^{2+}, Ca^{2+} and Zn^{2+} was studied with galvanostatic charge-discharge experiments. The electrodes were prepared by mixing different proportions of active materials, conductive carbon (Super P, Timcal) and polyvinylidene fluoride (PVDF) as the binder. Galvanostatic cycling measurements were done in three-electrode Swagelok cells using corresponding metal wire and foil as reference and counter electrode and suitable electrolyte to electrochemically strip and deposit the metal. Experiments were performed at room temperature for Mg and Zn, and at 100 °C for Ca cells. The current density was 10 $mA.g^{-1}$ for Mg and Zn and 5 $mA.g^{-1}$ for Ca. Detailed experimental conditions can be found in Table 2.

Table 2. Experimental conditions for electrochemical measurements.

Counter electrode	Electrode formulation: AM, C, PVDF Weight %	Electrolyte[5,8,15]
Mg	80 wt%, 10 wt%, 10 wt%	0.2 M 2PhMgCl-$AlCl_3$ / THF
Zn	70 wt%, 20 wt%, 10 wt%	0.5 M $Zn(TFSI)_2$ / acetonitrile
Ca	80 wt%, 10 wt%, 10 wt%	0.45 M $Ca(BF_4)_2$/ EC:PC (50:50 wt%)

Ex situ Synchrotron X-ray scattering. Electrochemically reduced/oxidized electrodes were washed with tetrahydrofuran or dimethyl carbonate and scrapped from the current collector and packed in kapton capillaries. Operations were performed in an Ar filled glove box. High energy X-ray (λ = 0.2128 Å) synchrotron diffraction data were collected at the 11-ID-B beamline at the Advanced Photon Source at Argonne National Laboratory. 1D diffraction data were obtained by integration of 2D total scattering data with Fit2D.[16] Pair Distribution Functions (PDF) were extracted using PDFgetX3.[17] The PDF refinements were performed using PDFgui[18].

Energy dispersive X-ray spectroscopy. EDX analysis was performed using a JEOL 2100 Plus transmission electron microscopy LaB6 200 kV.

Density function theory calculations. A lamellar lepidocrocite structure was simulated using a supercell made of two titanate layers (4x4x1 supercell) and two layers of interlayer water with an overall composition $Ti_{63}\square_1O_{124}(OH)_4{\cdot}32H_2O$ where the $\square$ represents a single Ti^{4+} vacancy whose charge is compensated by the four hydroxides. The spacing between titanate layers was fixed at 11.5 Å to be consistent with existing literature[19]. The simulation cell was computed using periodic boundary conditions. The choice to simplify the system was made to control for the role of the vacancy and to eliminate significant contributions from disorder in the structure. From this approach, this work will investigate the behaviour of intercalated multivalent ions (e.g. Mg^{2+}, Ca^{2+} and Zn^{2+}) and the structure and thermodynamics of stable structures in the vacancy and inter-layer positions.

Density functional theory (DFT) calculations were performed using the CP2K code via the Quickstep algorithm.[20,21] Electrons were described using the PBE exchange-correlation function with a planewave cut-off of 400 Rydberg. DZVP-MOLOPT-SR-GTH basis sets were used along with Goedecker-Teter-Hutter pseudopotentials[22,23]. Preliminary tests

using the Hubbard-U correction (U = 2.5 eV) were performed to understand the influence of correlation effects on energies of formations. A table summarizing these results can be found in the SI. DFT calculations in the article did not used the Hubbard-U correction as the differences in the computed energies of formation were on the order of 10meV/formula unit.

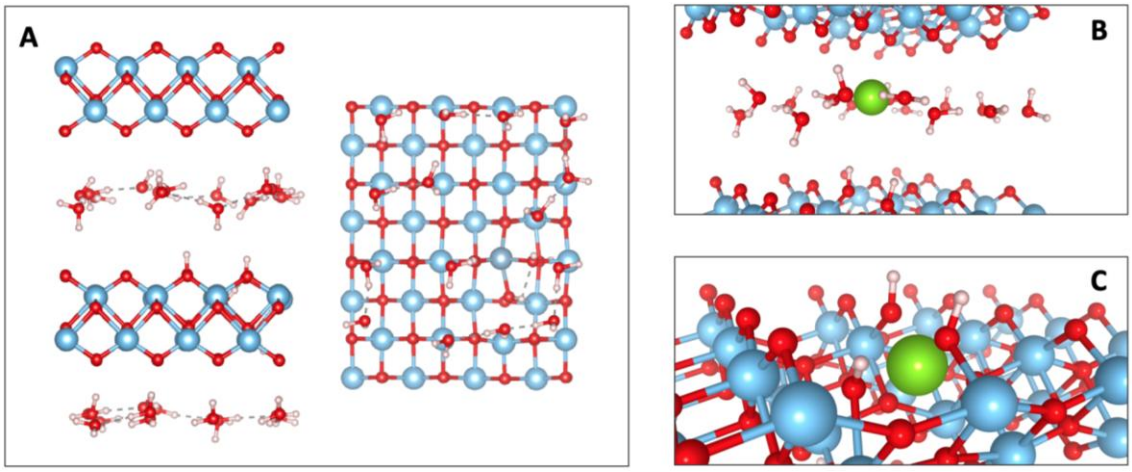

Figure 1. (A) The model lepidocrocite system considered here contains two titanate and two interlayer water layers. A single vacancy is introduced into one of the two titanate layers by removing a Ti atom and balancing the charge with four protons. Multivalent ions were inserted into one of two Wyckoff sites: the interlayer or the vacancy position (B) and (C) respectively, where the position of the multivalent ions is shown in green.

Given the size of the simulation cell, only the Γ-point was sampled. Systems are computed with a total neutral charge to simulate the state of the electrode following a discharge process.

Energy of Formation. Based on the Wyckoff positions, the energy of formation was computed for two different sites within the lepidocrocite structure: the ion in the water interlayer and the ion in the Ti^{4+} vacancy as shown in Figure 1B and C. To determine the energy of formation of the ion within the lepidocrocite structure, we relax the structure for the ion in each of the two previously mentioned positions allowing for both the ion and the electrode atoms to freely move. When this relaxed structure is determined, the total energy of the system is then recomputed for this arrangement of atoms but without the intercalated ion. The energy of formation is then computed via the formula:

$$E_f = E[X + TiO_2] - (E[X] + E[TiO_2])$$

where the first term represents the combined system and the terms in parentheses represent the sum of energies of the ion, X and titanate systems computed independently.

RESULTS AND DISCUSSION

Thermodynamic and analysis of the coordination environment of inserted-cations

The thermodynamic and coordination environment of each cation was probed by using DFT-calculations performed on a simplified structure, *i.e.*, a supercell $Ti_{63}\square_1O_{124}(OH)_4{\cdot}32H_2O$ where the □ represents a single Ti^{4+} vacancy whose charge is compensated by the four hydroxides, as shown in Figure 1. In both cases of the interlayer Wyckoff site (Figure 1B) and the cationic vacancy (Figure 1C), formation energies indicate that the intercalation reaction are thermodynamically favourable (Figure 2). We, however, note that zinc is the least stable ion within the two sites as compare to calcium and magnesium. We detailed below the structural features for each cation.

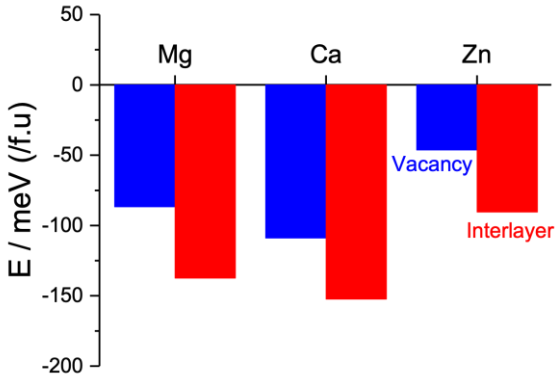

Figure 2. Energies of formation (meV/formula unit) for multivalent ions located in vacancy and interlayer Wyckoff positions in lepidocrocite-type TiO_2.

Magnesium. After completing the geometry relaxation, the magnesium ion is four-fold coordinated with water molecules (Figure 3A). The ion remains in the centre of the interlayer suggesting that the structure can remain stable upon Mg^{2+} insertion.

Within the vacancy (Figure 3D), Mg^{2+} ion is 6-fold coordinated with oxide anions with an average bond length of 2.06 Å. The ion is centred within the vacancy in almost exactly in the position one would expect for Ti^{4+}. As a result, there is only a small amount of distortion associated with the insertion of the ion into the vacancy site.

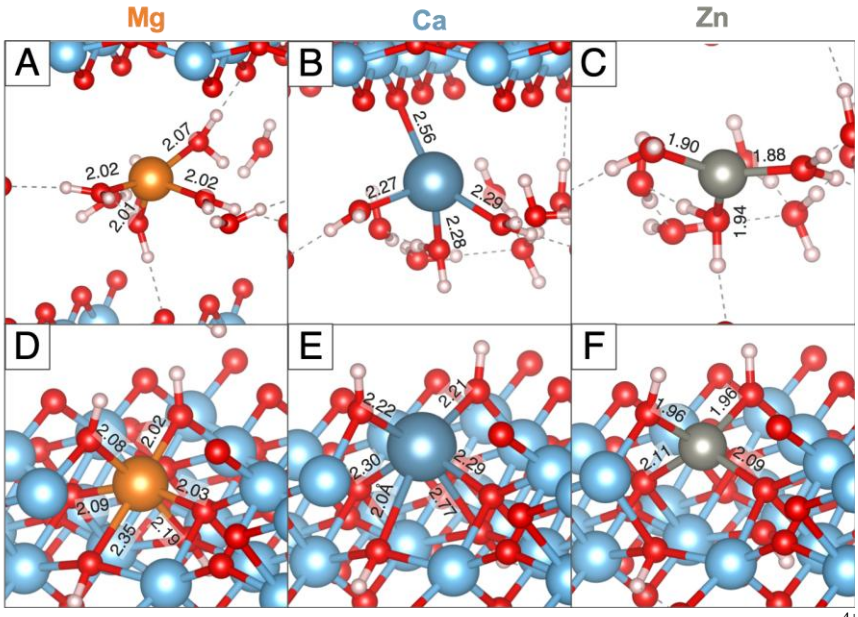

Figure 3. The relaxed geometries for Mg, Ca, and Zn ions in the water interlayer (A-C) and in the Ti^{4+} vacancy (D-F). Bond lengths are shown in units of Angstroms.

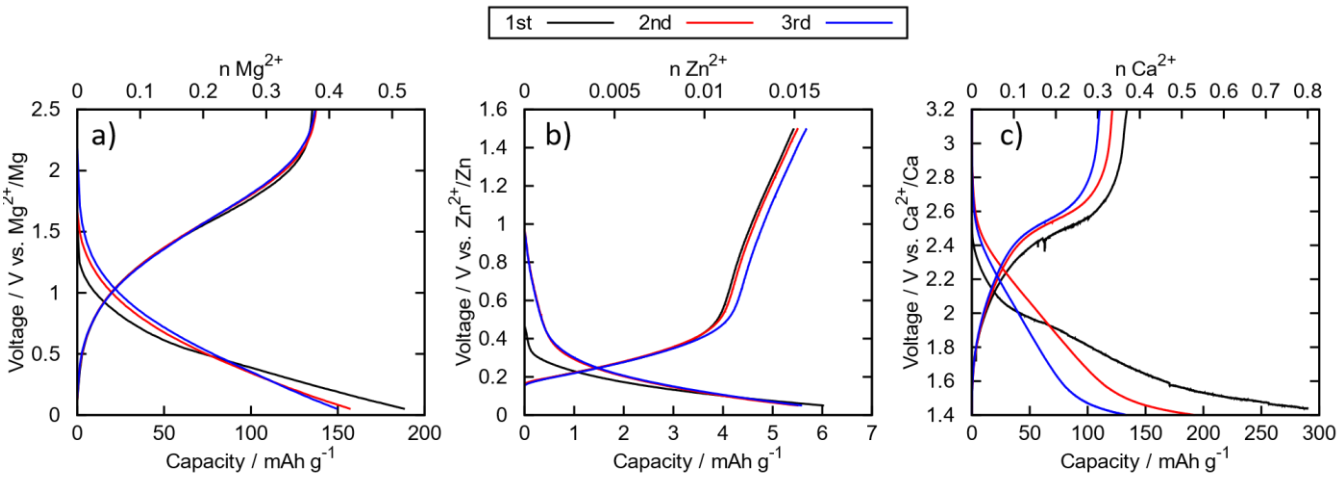

Figure 4. Galvanostatic discharge-charge curves in a) Mg, b) Zn and c) Ca cells. The used current densities were 10 $mA.g^{-1}$ for Mg^{2+} and Zn^{2+}, and 5 $mA.g^{-1}$ for Ca^{2+}.

Calcium. The relaxed structure computed for the interlayer calcium ion shows that the ion moved away from the centre of the interlayer. As a result, it is solvated by three water molecules and coordinated with a bridging oxygen from the titanate layer (Figure 3B). Such a configuration suggests that calcium insertion might destabilize the structure by moving water molecules away for the interlayer space. Within the vacancy, the ion forms four shorter bonds (~2.22 Å) and two longer bonds (~2.48 Å) (Figure 3E) effective coordination number[24] of 4.4. This is due to the position of the calcium ion with respect to the centre of the vacancy. Unlike the Mg^{2+}, which falls towards the centre of the vacancy, the larger size of Ca^{2+} induced a position farther away from the vacancy in the direction of the interlayer such that it is coordinated principally by the four outermost oxygen atoms. This destabilization as result of the distortion to the titanate structure has previously been observed in the case of K^+ in the lepidocrocite structure.[25]

Zinc intercalation. When intercalated into the interlayer, Zn^{2+} ion is three-fold coordinated by water molecules (Figure 3C). Similar to Mg^{2+} ion, zinc remains at the centre of the interlayer with no interactions with the titanate layer. When the ion is intercalated into the vacancy site, it sits higher than the centre of the void leading to a four-fold coordinated (Figure 3F), which is its preferred coordination number[26]. The four bonds formed with the Zn^{2+} have an average length of 2.07 Å with the two remaining oxygen atoms falling at 2.82/2.73 Å away from the ion. Such a configuration suggests an instability of Zn^{2+} to sit fully within the vacancy.

Electrochemistry. The electrode material that was used here consists of an amorphous compound featuring a local structure previously described using the layered lepidocrocite network. Disorder was suggested to be due to the large content of vacancies stabilized by the partial substitution of divalent O^{2-} by monovalent OH^- groups, *i.e.*, $Ti_{1.5}\square_{0.5}O_2(OH)_2{\cdot}nH_2O$ ($\square$ = Ti^{4+} vacancy, n~0.55).[14] The electrochemical properties of the lepidocrocite-type structure with respect to MV ions were assessed by employing the corresponding metal as the negative electrode. Moreover, specific electrolytes were chosen for

each system (Table 2). Figure 4 gathers galvanostatic charge/discharge curves obtained for the first three cycles. In the case of Mg^{2+}, the all-phenyl complex (APC) $Mg_2Cl_3^+AlPh_2Cl_2^-$ dissolved in tetrahydrofuran (THF) was used as the electrolyte. The voltage-composition (Figure 4a) curves measured at RT under 10 $mA.g^{-1}$, features a smooth profile suggesting a solid-solution behaviour. The reversible capacity was 135 mAh g^{-1} which corresponds to the intercalation of 0.37 Mg^{2+} per formula unit. Energy-dispersive x-ray spectroscopy was performed on a discharged electrode (Figure S1a) confirmed the insertion of naked Mg^{2+} with negligible amount of chloride (Cl/Ti = 0.02) ruling out the insertion of solvated species such as magnesium monochloride cations[27].

In the case of Zn^{2+} ions, the structure was shown to be electrochemically inactive (Figure 4b). The inability of the network to accommodate Zn^{2+} was confirmed by testing other type of solvent such as dimethyl sulfoxide. In the latter case, we measured very low capacities. The inability of Zn^{2+} to be inserted in the layered structure agrees with the thermodynamic reinforcing the observation of Zn as the least stable cation in the structure.

For Ca^{2+} intercalation, the selected electrolyte which was 0.45 M $Ca(BF_4)_2$/ EC:PC (50:50 wt%) requires to operate at 100 °C to provide an efficient plating/stripping of calcium.[5] Note that the thermal analysis showed that the structure is stable at this temperature.[14] The first discharge led to about 290 $mAh.g^{-1}$ (Figure 4c). EDX analysis performed on a discharge electrode indicated the presence of fluorine pointing to the decomposition of the boron fluoride groups from $Ca(BF_4)_2$ (Figure S1). The subsequent charge capacity reached 134 $mAh.g^{-1}$, corresponding to about 0.35 Ca^{2+} reversibly inserted per formula with an operating voltage of about 2.25V *vs.* Ca pseudo reference electrode. Large irreversible capacity is observed during the first few cycles assigned to the decomposition of the electrolyte and formation of a passivation layer containing calcium fluoride. Coulombic efficiency above 98% is reached only after 5 cycles (Figure S2), which is probably due to the progressive decomposition of the electrolyte and formation of CaF_2-based layer.

Intercalation mechanisms. The intercalation mechanisms of Mg^{2+} and Ca^{2+} within the lepidocrocite structure were investigated using the pair distribution function. Such a method obtained by the Fourier transformation of high-energy x-ray data, enables to get structural information of x-ray amorphous compounds.[28] Figure 5 gathered the PDFs of the pristine, discharged and charged electrodes *vs.* Mg^{2+}/Mg. The PDF of the pristine electrode presents peaks whose intensities gradually decrease and vanish at inter-atomic distances that are greater than 10 Å, which is a characteristic of x-ray amorphous compounds.

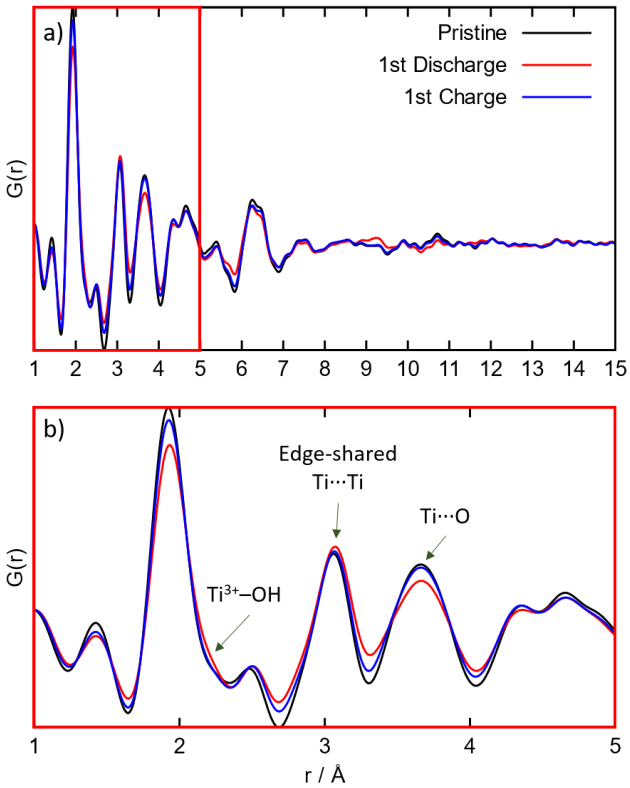

Figure 5. Ex-situ X-ray atomic pair distribution function of pristine, fully discharged and fully charged sample *vs.* Mg^{2+}/Mg, a) extended and b) zoomed view.

The insertion and subsequent de-insertion of Mg^{2+} produced minor changes to the PDFs suggesting that the local structure is maintained upon (de)-intercalation. Upon Mg^{2+} insertion, the intensity of the first peak characteristic of Ti-O(H) bond distances decreased while a small shoulder at 2.16 Å appears, which is assigned to reduced Ti^{3+}-O(H) bonds. This implies that the redox activity at titanium sites is a consequence of the Ti^{4+}/T^{i3+} redox couple. Moreover, the second peak at 3.1 Å can be assigned to edge-shared Ti···Ti bonds and the third peak at 3.65 Å can be attributed to Ti···O distances broaden upon Mg^{2+} insertion, which can be due to the appearance of reduced Ti^{3+}-O(H) and Mg-O(H) bonds. Small features can be observed at higher inter-atomic distances, *i.e.*, ~9 Å, suggesting that the Mg^{2+} intercalation produced changes up to the intermediate range-order, ruling out capacitive contributions.

We further attempted to refine the PDF data using a disordered lepidocrocite structure (Figure S3). The results, however, was not conclusive, particularly in discriminating any sort of site preferences for Mg-ions. It can be postulated that Mg^{2+} can be inserted at both sites, and the populations in each site is a result of the relative stability the ion experiences either via the solvation of water molecules or within the titanate layer. We also note that Mg^{2+} insertion take place without solvated chloride-based species.

Upon subsequent Mg^{2+} de-intercalation, the peaks match those of the pristine showing that Mg^{2+} insertion proceeds in a reversible manner. We note that even at the intermediate range-order, the peaks match their initial position. The network stability upon Mg^{2+} intercalation/de-intercalation primary suggests that water molecules remain in the interlayer space and does not shuttle into the electrolyte. The precise role of

interlayer water molecules during Mg^{2+} intercalation and de-intercalation in 2D hydrated structure is still challenging to establish.[29–33] In particular, the structure stability upon extended cycling would need a deeper investigation.

To better understand Mg^{2+} intercalation within the lepidocrocite structure, we compared the energy of formation for several positions of the ion throughout the structure of the computed supercell $Ti_{63}\square_1O_{124}(OH)_4{\cdot}32H_2O$. As shown by a dotted line in Figure 6, a path perpendicular to the titanate layer passing between water interlayers via the titanium vacancy was considered. At each position of the ion along this path, the structure was allowed to relax to find a local energy minimum. Thus, the profile of energies in Figure 6 should not be taken as the diffusion pathway of ions, but a series of local minima computed to provide insight into the interaction between the ions and the host material. We compare the two profiles for Li^+ and Mg^{2+}, highlighting three positions along the ion path: in the titanium vacancy (Position A), just outside the vacancy (Position B), and in the interlayer (Position C). To better compare the energy of formation profiles between ions, Figure 6 shows the difference in the energy of formation (ΔE) with respect to the lowest computer energy formation along the path. For each ion, the lowest energy of formation was determined to be in the interlayer position. It should be noted that an increase in the profile represents relative stability amongst the varying positions. Energies of formation remain favourable, as was shown in Figure 2. Moreover, we expected the diffusion of Mg^{2+} to be more favourable in the disordered material, particularly when approaching the titanate layer, *i.e.*, when the formation energy increases drastically. The profiles at the three noted positions, do not vary significantly, although most notable at position B (~0.72eV). This position, corresponding to the ion just outside of the vacancy, looks structurally similar between the two ions. In each case, the ion prefers to move out of the plane between the two hydroxyl groups, minimizing the amount of distortion that is experienced within the structure. The distance between the hydroxyl groups in the relaxed structures were 3.69Å and 3.67 Å for Li^+ and Mg^{2+} respectively. The similarity in these distances suggests that the difference in energy is not likely due to differing amounts of distortion induced by the ions themselves, and we thus conclude that the polarizing power of the ion is likely the main driving force in the energetic penalty of the magnesium ion.

As opposed to Mg^{2+}, the insertion of Ca^{2+} induced a drastic structural change. X-ray diffraction analysis (Figure S1) of the discharged electrode revealed the presence of a crystallized compound attributed to CaF_2 (S.G: Fm-3m) and weak peaks tentatively assigned to $CaB_3O_4(OH)_4H_2O$[34]. Both phases indicate the degradation of the electrolyte. The PDF of the discharged electrode (Figure 7a) showed peaks beyond 10 Å, which can be attributed to the presence of newly formed crystallized phases. Moreover, for low *r* region, the peak located at 3.1 Å assigned to edge-shared Ti···Ti bond distances disappeared, suggesting a phase change with new atoms connectivity's formed upon Ca^{2+} insertion. The disappearance of edge-shared Ti···Ti connectivities indicated that the layer structure was not maintained and therefore, that water molecules were released in the electrolyte. This is supported by the large content of CaF_2 observed by XRD, whose formation can be promoted by the hydrolysis of BF_4^- groups releasing fluoride ions[35].

To understand the structural changes induce by Ca^{2+} insertion, we attempted to refine the PDF data with the following procedure: (i) we refined the data by excluding the short-range order (i.e., for $r > 7$ Å). For 7-30 Å, the PDF was well reproduced by using CaF_2 as a structural model. Subsequently, we fixed all the parameters and refined the data from 1 to 20 Å (Figure 7b), which revealed inter-atomic distances that can be assigned to the newly formed phase. Such a phase features only a short-range order. We tentatively assigned the most intense peaks at 1.94 Å to Ti-O bonds, at 2.3 Å to Ca-O bonds and at 3.8 Å to corner-shared Ti···Ti. Considering the absence of edge-shared Ti···Ti connectivities, we deduced from the ICSD database that the newly formed phase has a local perovskite-like structure as found in $CaTiO_3$[36], a structure where Ca^{2+} is 7-fold coordinated (Inset Figure 7d), which is close to its preferred 8-fold coordination number[9,26]. The calculated PDF of $CaTiO_3$ **(**Figure S2**)** is, however, characterized by an intense peak at 3.2 Å assigned to Ca···Ti connectivities. The weak presence of this peak in the newly formed phase suggested an under stoichiometry in Ca^{2+}. The exact chemical formula is, however, not trivial to determine. We simulated the PDF of $CaTiO_3$ (Figure 7c) featuring low content of Ca (Ca occupancy = 0.34) and found that it matches the experimental data with a PDF scattering domain length of around 8 Å highlighting strong disorder. The newly formed phase enabled to insert Ca^{2+} in a reversible manner. Our work confirms that disordered perovskite-based structure could be seen as an attractive framework to enable practical Ca-batteries.[37]

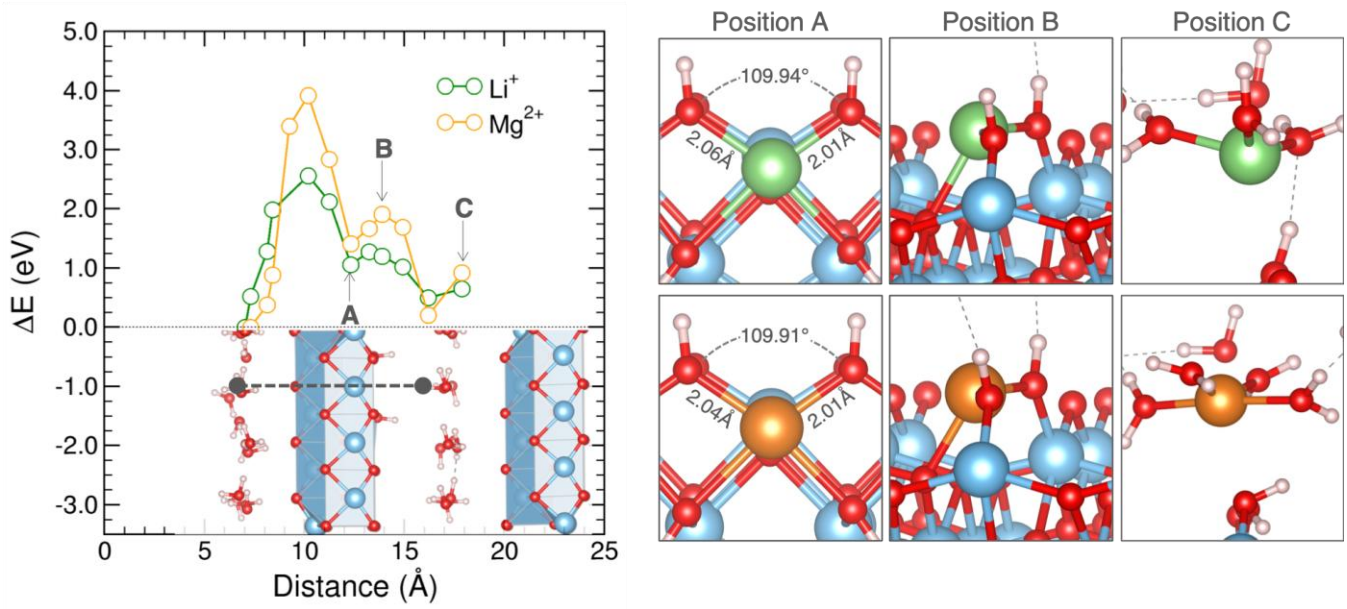

Figure 6. Change in the energy of formation for Li^+ (green) and Mg^{2+} (orange) ions in the lepidocrocite structure. Relaxed geometries are visualized at the vacancy structure (A), having just left the titanium vacancy (B), and the water interlayer (C). The energy of formation profile corresponding to a path between interlayers, shown as a dotted black line.

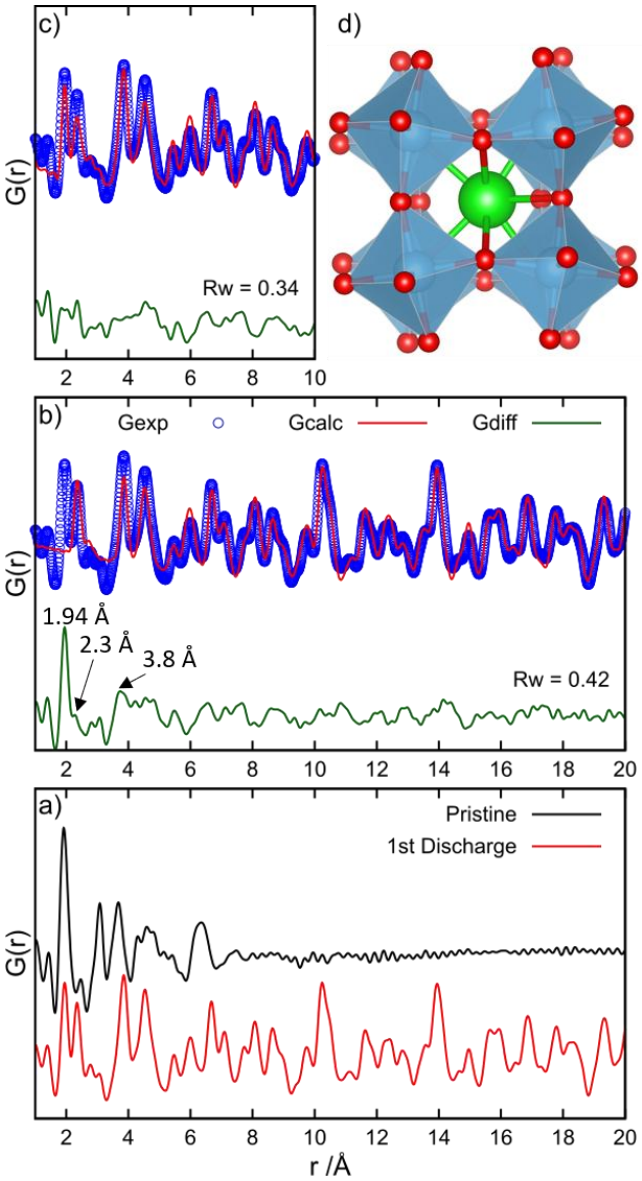

Figure 7. a) X-ray PDFs of pristine and fully discharged electrode *vs.* Ca^{2+}/Ca. b) refinement of the PDF data using CaF_2 (S.G. Fm-3m) as a structural model and c) using CaF_2 and Ca_xTiO_3 (S.G. Pbnm) perovskite structure, d) Polyhedral representation of the perovskite structure.

CONCLUSION

We investigated the electrochemical properties *vs.* multivalent ions (Mg^{2+}, Zn^{2+}, Ca^{2+}) of a disordered layered type structure featuring water-containing interlayer and titanium vacancies ($Ti_{1.5}\square_{0.5}O_2(OH)_2{\cdot}nH_2O$). First-principle calculations were primary performed on a simplified supercell $Ti_{63}\square_1O_{124}(OH)_4{\cdot}32H_2O$ to assess the thermodynamics of ions intercalation reaction within either the interlayer space or titanium vacancy. Despite favourable formation energies, experimental data showed drastic differences between ions due to their intrinsic properties (size, polarizing power) and operating conditions (temperature, electrolyte). Galvanostatic experiments showed that Zn^{2+} cannot be intercalated within the lepidocrocite-type structure possibly due to unfavorable arrangement within the vacant sites as revealed by first-principle calculations. In the case of magnesium, the structure is able to reversibly intercalated 0.37 Mg^{2+} per chemical formula. Pair distribution function computed for the discharged and charged electrodes demonstrated that the layered framework is maintained. We suggest that this is due to only slight distortions to the titanate structure as predicted by geometry relaxations and due to interlayer water maintaining its role of structural stabilization during the insertion of Mg^{2+}. Moreover, unsolvated Mg^{2+} ions are inserted as demonstrated by EDX analysis showing the absence of chlorine, ruling out the insertion of magnesium chlorinated species. The electrochemical insertion of Ca^{2+} induced the collapse of the layered structure with the release of the interlayer water molecules that contributed to the degradation of the electrolyte as shown by the formation of CaF_2. The refinement of the pair distribution function measured on the discharged electrode indicated that the newly formed phase, which is electrochemically active, featured strong disorder and short-range order close to those found in perovskite structure, particularly with corner-shared TiO_6 octahedra. Perspectives in synthetizing defective $CaTiO_3$-based perovskite could be explored to identify viable cathode materials for rechargeable Ca-based batteries.

ASSOCIATED CONTENT

Supporting Information

AUTHOR INFORMATION

Corresponding Author

* damien.dambournet@sorbonne-universite.fr

Author Contributions

‡These authors contributed equally.

Funding Sources

The research leading to these results has received funding from the French National Research Agency under Idex@Sorbonne University for the Future Investments program (no. ANR-11-IDEX-0004-02). Funding from the European Union's Horizon 2020 research is acknowledged: European Research Council (ERC-2016-STG, CAMBAT grant agreement No 715087).

ACKNOWLEDGMENT

The work done at the Advanced Photon Source, an Office of Science User Facility operated for the U.S. Department of Energy (DOE) Office of Science by Argonne National Laboratory, was supported by the U.S. DOE under contract no. DE-AC02-06CH11357. A. Ponrouch is grateful to the Spanish Ministry for Economy, Industry and Competitiveness Severo Ochoa Programme for Centres of Excellence in R&D (SEV-2015-0496). We thank IMPC FR2482 for SEM-FEG and TEM instrumentation funded by CNRS, Sorbonne Université and C'Nano projets of Region Ile-de-France.

REFERENCES

(1) Kubota, K.; Dahbi, M.; Hosaka, T.; Kumakura, S.; Komaba, S. Towards K-Ion and Na-Ion Batteries as "Beyond Li-Ion." *Chem. Rec.* **2018**.

(2) Muldoon, J.; Bucur, C. B.; Gregory, T. Quest for Nonaqueous Multivalent Secondary Batteries: Magnesium and Beyond. *Chem. Rev.* **2014**, *114* (23), 11683–11720.

(3) Canepa, P.; Sai Gautam, G.; Hannah, D. C.; Malik, R.; Liu, M.; Gallagher, K. G.; Persson, K. A.; Ceder, G. Odyssey of Multivalent Cathode Materials: Open Questions and Future Challenges. *Chem. Rev.* **2017**, *117* (5), 4287–4341.

(4) Aurbach, D.; Lu, Z.; Schechter, A.; Gofer, Y.; Gizbar, H.; Turgeman, R.; Cohen, Y.; Moshkovich, M.; Levi, E. Prototype Systems for Rechargeable Magnesium Batteries. *Nature* **2000**, *407* (6805), 724–727.

(5) Ponrouch, A.; Frontera, C.; Bardé, F.; Palacín, M. R. Towards a Calcium-Based Rechargeable Battery. *Nat. Mater.* **2016**, *15* (2), 169–172.

(6) Arroyo-de Dompablo, M. E.; Ponrouch, A.; Johansson, P.; Palacín, M. R. Achievements, Challenges, and Prospects of Calcium Batteries. *Chem. Rev.* **2019**, acs.chemrev.9b00339.

(7) Konarov, A.; Voronina, N.; Jo, J. H.; Bakenov, Z.; Sun, Y.-K.; Myung, S.-T. Present and Future Perspective on Electrode Materials for Rechargeable Zinc-Ion Batteries. *ACS Energy Lett.* **2018**, *3* (10), 2620–2640.

(8) Han, S.-D.; Rajput, N. N.; Qu, X.; Pan, B.; He, M.; Ferrandon, M. S.; Liao, C.; Persson, K. A.; Burrell, A. K. Origin of Electrochemical, Structural, and Transport Properties in Nonaqueous Zinc Electrolytes. *ACS Appl. Mater. Interfaces* **2016**, *8* (5), 3021–3031.

(9) Rong, Z.; Malik, R.; Canepa, P.; Sai Gautam, G.; Liu, M.; Jain, A.; Persson, K.; Ceder, G. Materials Design Rules for Multivalent Ion Mobility in Intercalation Structures. *Chem. Mater.* **2015**, *27* (17), 6016–6021.

(10) Canepa, P.; Sai Gautam, G.; Hannah, D. C.; Malik, R.; Liu, M.; Gallagher, K. G.; Persson, K. A.; Ceder, G. Odyssey of Multivalent Cathode Materials: Open Questions and Future Challenges. *Chem. Rev.* **2017**, *117* (5), 4287–4341.

(11) Cui, L.; Zhou, L.; Kang, Y.-M.; An, Q. Recent Advances in the Rational Design and Synthesis of Two-Dimensional Materials for Multivalent Ion Batteries. *ChemSusChem* **2020**, *13* (6), 1071–1092.

(12) Koketsu, T.; Ma, J.; Morgan, B. J.; Body, M.; Legein, C.; Dachraoui, W.; Giannini, M.; Demortière, A.; Salanne, M.; Dardoize, F.; Groult, H.; Borkiewicz, O. J.; Chapman, K. W.; Strasser, P.; Dambournet, D. Reversible Magnesium and Aluminium Ions Insertion in Cation-Deficient Anatase TiO_2. *Nat. Mater.* **2017**, *16* (11), 1142.

(13) Orikasa, Y.; Kisu, K.; Iwama, E.; Naoi, W.; Yamaguchi, Y.; Yamaguchi, Y.; Okita, N.; Ohara, K.; Munesada, T.; Hattori, M.; Yamamoto, K.; Rozier, P.; Simon, P.; Naoi, K. Noncrystalline Nanocomposites as a Remedy for the Low Diffusivity of Multivalent Ions in Battery Cathodes. *Chem. Mater.* **2020**.

(14) Ma, J.; Reeves, K. G.; Porras Gutierrez, A.-G.; Body, M.; Legein, C.; Kakinuma, K.; Borkiewicz, O. J.; Chapman, K. W.; Groult, H.; Salanne, M.; Dambournet, D. Layered Lepidocrocite Type Structure Isolated by Revisiting the Sol–Gel Chemistry of Anatase TiO2: A New Anode Material for Batteries. *Chem. Mater.* **2017**, *29* (19), 8313–8324.

(15) Song, J.; Sahadeo, E.; Noked, M.; Lee, S. B. Mapping the Challenges of Magnesium Battery. *J. Phys. Chem. Lett.* **2016**, *7* (9), 1736–1749.

(16) Hammersley, A. P.; Svensson, S. O.; Hanfland, M.; Fitch, A. N.; Hausermann, D. Two-Dimensional Detector Software: From Real Detector to Idealised Image or Two-Theta Scan. *High Press. Res.* **1996**, *14* (4–5), 235–248.

(17) Juhás, P.; Davis, T.; Farrow, C. L.; Billinge, S. J. L. PDFgetX3 : A Rapid and Highly Automatable Program for Processing Powder Diffraction Data into Total Scattering Pair Distribution Functions. *J. Appl. Crystallogr.* **2013**, *46* (2), 560–566.

(18) Farrow, C. L.; Juhas, P.; Liu, J. W.; Bryndin, D.; Božin, E. S.; Bloch, J.; Proffen, T.; Billinge, S. J. L. PDFfit2 and PDFgui: Computer Programs for Studying Nanostructure in Crystals. *J. Phys. Condens. Matter* **2007**, *19* (33), 335219.

(19) Yuan, H.; Besselink, R.; Liao, Z.; ten Elshof, J. E. The Swelling Transition of Lepidocrocite-Type Protonated Layered Titanates into Anatase Under Hydrothermal Treatment. *Sci. Rep.* **2014**, *4*.

(20) Hutter, J.; Iannuzzi, M.; Schiffmann, F.; Vandevondele, J. CP2K: Atomistic Simulations of Condensed Matter Systems. *WIREs Comput. Mol. Sci.* **2014**, *4*, 15–25.

(21) VandeVondele, J.; Krack, M.; Mohamed, F.; Parrinello, M.; Chassaing, T.; Hutter, J. Quickstep: Fast and Accurate Density Functional Calculations Using a Mixed Gaussian and Plane Waves Approach. *Comput. Phys. Commun.* **2005**, *167* (2), 103–128.

(22) VandeVondele, J.; Hutter, J. Gaussian Basis Sets for Accurate Calculations on Molecular Systems in Gas and Condensed Phases. *J. Chem. Phys.* **2007**, *127* (11), 114105.

(23) Goedecker, S.; Teter, M.; Hutter, J. Separable Dual-Space Gaussian Pseudopotentials. *Phys. Rev. B* **1996**, *54* (3), 1703–1710.

(24) Momma, K.; Izumi, F. VESTA 3 for Three-Dimensional Visualization of Crystal, Volumetric and Morphology Data. *J. Appl. Crystallogr.* **2011**, *44* (6), 1272–1276.

(25) Reeves, K. G.; Ma, J.; Fukunishi, M.; Salanne, M.; Komaba, S.; Dambournet, D. Insights into Li+, Na+, and K+ Intercalation in Lepidocrocite-Type Layered TiO2 Structures. *ACS Appl. Energy Mater.* **2018**, *1* (5), 2078–2086.

(26) Brown, I. D. What Factors Determine Cation Coordination Numbers? *Acta Crystallogr. B* **1988**, *44* (6), 545–553.

(27) Yoo, H. D.; Liang, Y.; Dong, H.; Lin, J.; Wang, H.; Liu, Y.; Ma, L.; Wu, T.; Li, Y.; Ru, Q.; Jing, Y.; An, Q.; Zhou, W.; Guo, J.; Lu, J.; Pantelides, S. T.; Qian, X.; Yao, Y. Fast Kinetics of Magnesium Monochloride Cations in Interlayer-Expanded Titanium Disulfide for Magnesium Rechargeable Batteries. *Nat. Commun.* **2017**, *8* (1), 1–10.

(28) Billinge, S. J. L.; Kanatzidis, M. G. Beyond Crystallography: The Study of Disorder, Nanocrystallinity and Crystallographically Challenged Materials with Pair Distribution Functions. *Chem. Commun.* **2004**, No. 7, 749–760.

(29) Tepavcevic, S.; Liu, Y.; Zhou, D.; Lai, B.; Maser, J.; Zuo, X.; Chan, H.; Král, P.; Johnson, C. S.; Stamenkovic, V.; Markovic, N. M.; Rajh, T. Nanostructured Layered Cathode for Rechargeable Mg-Ion Batteries. *ACS Nano* **2015**, *9* (8), 8194–8205.

(30) Sa, N.; Kinnibrugh, T. L.; Wang, H.; Sai Gautam, G.; Chapman, K. W.; Vaughey, J. T.; Key, B.; Fister, T. T.; Freeland, J. W.; Proffit, D. L.; Chupas, P. J.; Ceder, G.; Bareno, J. G.; Bloom, I. D.; Burrell, A. K. Structural Evolution of Reversible Mg Insertion into a Bilayer Structure of V2O5·nH2O Xerogel Material. *Chem. Mater.* **2016**, *28* (9), 2962–2969.

(31) Ji, X.; Chen, J.; Wang, F.; Sun, W.; Ruan, Y.; Miao, L.; Jiang, J.; Wang, C. Water-Activated VOPO4 for Magnesium Ion Batteries. *Nano Lett.* **2018**, *18* (10), 6441–6448.

(32) Sai Gautam, G.; Canepa, P.; Richards, W. D.; Malik, R.; Ceder, G. Role of Structural H2O in Intercalation Electrodes: The Case of Mg in Nanocrystalline Xerogel-V2O5. *Nano Lett.* **2016**, *16* (4), 2426–2431.

(33) Tan, S.; Xiong, F.; Wang, J.; An, Q.; Mai, L. Crystal Regulation towards Rechargeable Magnesium Battery Cathode Materials. *Mater. Horiz.* **2020**. https://doi.org/10.1039/D0MH00315H.

(34) Hainsworth, F. N.; Petch, H. E. The Structural Basis of Ferroelectricity in Colemanite. *Can. J. Phys.* **1966**, *44* (12), 3083–3107.

(35) Freire, M. G.; Neves, C. M. S. S.; Marrucho, I. M.; Coutinho, J. A. P.; Fernandes, A. M. Hydrolysis of Tetrafluoroborate and Hexafluorophosphate Counter Ions in Imidazolium-Based Ionic Liquids. *J. Phys. Chem. A* **2010**, *114* (11), 3744–3749.

(36) Sasaki, S.; Prewitt, C. T.; Bass, J. D.; Schulze, W. A. Orthorhombic Perovskite CaTiO3 and CdTiO3: Structure and Space Group. *Acta Crystallogr. Sect. C* **1987**, *43* (9), 1668–1674.

(37) Torres, A.; Luque, F. J.; Tortajada, J.; Arroyo-de Dompablo, M. E. DFT Investigation of Ca Mobility in Reduced-

Perovskite and Oxidized-Marokite Oxides. *Energy Storage Mater.* **2019**, *21*, 354–360.